Body and wake influences on the 3D flow close to a HAWT rotor

Daniel Micallef[*], Buşra Akay[†], Tonio Sant[‡], Carlos Simão Ferreira[§], and Gerard van Bussel[¶]

Abstract

This work focuses on the hypothesis that flow three-dimensionality in the rotor proximity is strongly affected by blade blockage and bound circulation.

The extent of flow three-dimensionality in the blade proximity needs to be assessed particularly in sensitive regions such as the root and tip of the blade. Moreover the induction needs to be decomposed into two components; that resulting due to the blade presence and that due to the wake. In this regard, the estimation of bound vorticity is essential such that its effects and those due to trailing vorticity can be understood.

To investigate the hypothesis, an experimental and a numerical approach is used. A two bladed, 2m diameter rotor was tested in the Open Jet Facility at TU Delft measuring 6m×6.5m×13.5m using Stereo Particle Image Velocimetry (SPIV).

The flow field around the tested HAWT blade was successfully measured and the velocity components around the entire blade were studied. The bound vorticity was measured using the experimental data and compared well with the numerical measurements. The radial flow, responsible for 3D effects was found to have high values not at the 100% span position but rather at around 90% span. The flow components were also decomposed using the potential flow model. Whilst the wake causes an increase in the flow three-dimensionality, the blade effect was found to be indeed the opposite and hence to decrease the inductions (and hence flow three-dimensionality).

While momentum approaches utilize correction functions to account for the finite nature of the HAWT blade, we provide new understanding of the three-dimensional flow field which may prove useful for future work in refining momentum formulations.

1 Introduction

Well established methods such as blade element momentum (BEM) theory are purely based on a 2D formulation using a conservation of momentum in the axial and azimuthal direction. BEM approaches usually take account of the difference between local and azimuthally averaged inductions by means of a tip loss factor. The most common of these corrections is that by Prandtl as reported by Betz [1]. In his model however, the finite blade effect is modelled by means of a series of discs carrying vorticity which represent the wake only. Contradicting this statement is the fact that a HAWT blade carries bound vorticity which distorts the flow field and hence the local induction at the blades. Based on this observation we hypothesize that local body effects can have a substantial influence on the flow in the blade vicinity particularly in sensitive regions such as the tip. The objective of this paper is to quantify the effect of induction of the wake against the effect of induction of the body. In this regard we address the following research questions:

[*]PhD researcher, TUDelft and University of Malta. d.micallef@tudelft.nl
[†]PhD researcher, TUDelft. b.akay@tudelft.nl
[‡]Senior Lecturer, University of Malta. tonio.sant@um.edu.mt
[§]Assistant Professor, TUDelft. C.J.SimaoFerreira@tudelft.nl
[¶]Professor, TUDelft. G.J.W.vanBussel@tudelft.nl

1. How does the flow around the blade behave?

2. How do the body and wake contribute?

In order to test our hypothesis we used a 3D unsteady potential-flow panel model. To validate and support the analysis, experimental measurements in the rotor plane were required. For this reason, a 2m diameter two-bladed wind turbine model was tested in the Open Jet Facility (OJF) at Delft University of Technology. Stereo Particle Image Velocimetry (SPIV) was used to determine the velocity field close to the blades. The experiment was simulated using the 3D unsteady, potential-flow panel model. The numerical simulations were validated with the experimental data and used to analyze the causes of flow three-dimensionality around wind turbine blades.

Flow velocities were measured in past experiments using SPIV as well as hot-wire anemometry. In the NREL Unsteady Aerodynamics Experiment (UAE) (refer to Hand et al.[2]) the flow velocities where not measured directly since only pressure measurements were performed. Most of the insight on flow velocities were obtained by means of numerical modelling ranging from lifting-line vortex models such as by Sant et al. [3] to 3D Navier Stokes modelling (Uzol et al. [4]). In the case of lifting-line vortex models, the blade's physical geometry is not modelled and no insight can be gained on the flow around it. Maast et al. [5] discuss the effects of blade thickness on the flow field in the blade's vicinity but no detailed analysis was given. Full Navier Stokes models on the other hand can give good insight on the flow around the blade. However, there is currently a lack of experimental data which can be used to validate these more advanced numerical techniques. Various other experimental studies have been conducted which report velocities in the wake such as by Medici et al.[6] at locations 1D downstream. Ebert et al. [7, 8, 9] show the velocity components at around 1.5 chord lengths downstream and the tip vortex was found to have a relatively high impact in the tip region. These research efforts however do not give any information on the flow in the blade vicinity. Maeda et al. [10] calculated bound vorticity using Laser Doppler Velocimetry (LDV) at various blade sections on a 2.4m, three-bladed turbine. Not much is however discussed on the flow three-dimensionality on the blade.

Flow field measurements have also been performed in the Model Experiment in Controlled Conditions (MEXICO) (see Schepers et al. [11]) using Stereo Particle Image Velocimetry (SPIV). The experiment was performed using a three bladed, 4.5m diameter rotor model in the German-Dutch wind tunnel (DNW) with an open jet test cross section of 9.5 m x 9.5 m. Both axial as well as yawed flow measurements were carried out. Results for the flow velocities were obtained in the MEXNEXT project but this work is not yet published at the time of writing of this paper. The MEXICO rotor was also simulated such that we extend our conclusions to blades having substantially different geometries.

2 Experiment Description

In the SPIV experiment, the wind turbine model was tested in the OJF wind tunnel at TU Delft which has an octagonal jet exit with a 3m equivalent diameter. The test section measures 6m×6.5m×13.5m. Figure 1 shows the chord and twist distributions of the blade. The airfoil section used was a DU96-W180 throughout the entire span of the blade except at the connection point with the hub (nacelle). The tip radius was 1 m while the root radius was 0.147 m. The rotor had two blades and rotated in a clock-wise direction when looking downwind.

The equipment used is listed here:

- 16 mega-pixel digital cameras

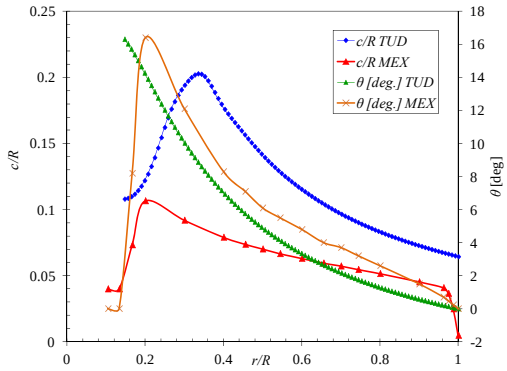

Figure 1: Twist and chord distribution along the TU Delft and MEXICO blades.

- 180mm lenses
- Double cavity pulsed Nd:Yag laser
- Automated traverse system
- Smoke seeding

The test conditions are summarized in tab. 1. Thirty measurement planes where taken along the blade span with 30mm increments from root to tip. For each of the measurement planes, 75 phase locked image couples were taken from both cameras such that the mean flow velocities can then be averaged. The measurement plane is indicated in figure 3. The field of view for each plane was 290mm×199mm. A 50% window overlap and multi-pass refinement were used in the processing of the images.

The MEXICO rotor measured 4.5m diameter and consisted of three blades. The experiment was performed in the German-Dutch wind tunnel (DNW) having an open jet test cross section of 9.5 m x 9.5 m. The campaign involved pressure measurements at five spanwise stations and also SPIV measurements at the rotor plane and at various downstream positions. Measurements were carried out for both axial and yawed flow. The experimental conditions used in this study are also given in tab. 1. Further details can be found in Schepers et al. [11]. The blade had 3 different airfoil sections along the span; a DU91-W2-250 at the root region, RisøA1-21 at the mid-board region and a NACA 64418 at the tip region. The chord and twist distribution are also given in Figure 1.

3 Numerical methodology

The experimental turbine was modelled using a 3D unsteady potential-flow panel-method with a free-wake model as described by Katz and Plotkin [12]. To model a 3D body, the surface is approximated by a number of doublet and source panels. As the blades rotate, a wake of free-convecting doublets is released from the trailing edge. The panel model uses a Dirichlet boundary condition. This can then be used to evaluate the velocities by means of differentiating the potential function given by (Katz and Plotkin [12]):

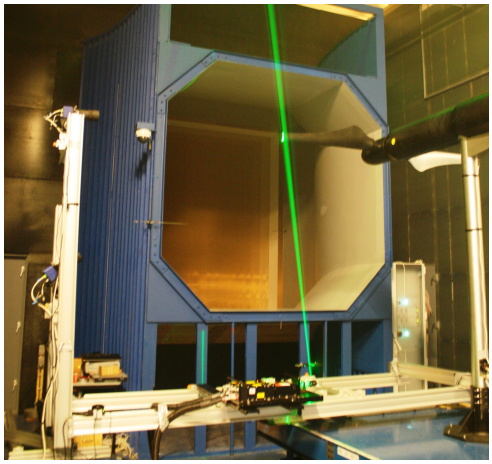

Figure 2: Photograph showing setup configuration.

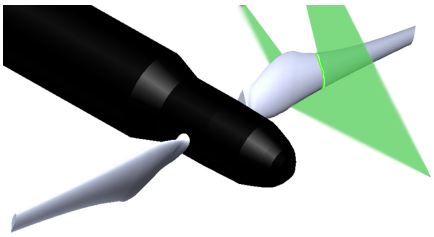

Figure 3: Measurement plane positioned with respect to the horizontal blade. The plane is moved along the span with increments of 30mm.

$$\nabla\Phi = -\frac{1}{4\pi}\int_{S_B}\sigma\nabla\left(\frac{1}{x}\right)ds + \frac{1}{4\pi}\int_{S_B+S_W}\mu\nabla\left[\frac{\partial}{\partial n}\left(\frac{1}{x}\right)\right]dS + \nabla\Phi_\infty \tag{1}$$

Figure 4 represents the body having doublet strengths μ_u and μ_l on the suction and pressure side of the airfoil respectively. Source terms on the upper and lower surfaces should also be included but are not shown in the figure to keep it uncluttered. According to the Kutta condition, the vorticity at the trailing edge should be zero. Thus, the wake doublet strength is given by the difference in doublet strengths of the upper and lower surfaces of the body. The model may be used to simulate the behaviours of multiple bodies such as for instance the blades, nacelle and tower. The formulation used in this model is an unsteady approach and therefore can account for unsteady effects. A more detailed treatment is given in Katz and Plotkin [12]. Thorough validation of the model was carried out by Dixon [13] and Ferreira [14].

The input parameters for the very fine mesh simulation are summarized in tab. 2. The operating conditions of wind speed and rotor speed mentioned in tab. 1 were used as input.

The MEXICO rotor and nacelle were also simulated with the same numerical model. The simulation was performed for a tip speed ratio of 6.67 with a wind speed of 15m/s and 424.5RPM. The discretization of the bodies into panels is shown in tab. 2. Since the MEXICO rotor was three bladed, three wake sheets have to be computed for which increases the number of panels and hence the computation time. A similar verification study as for the TU Delft rotor simulation was also performed to ensure convergence of the final solution.

Table 1: Experimental condition specifications for the TU Delft and the MEXICO experiment. *Note: Thrust coefficient and power coefficient quoted as obtained from momentum theory. Quoted thrust and power coefficients are those from the simulations. For the MEXICO rotor, experimental results give $C_T = 0.72$ and $C_P = 0.377$.

	TU Delft	MEXICO
Yaw angle[°]	0	0
Wind speed [m/s]	6	15
Pitch[°]	0	-2.3
Tip speed ratio	7	6.7
Thrust coefficient	0.783	0.875*
Power coefficient	0.45	0.358*

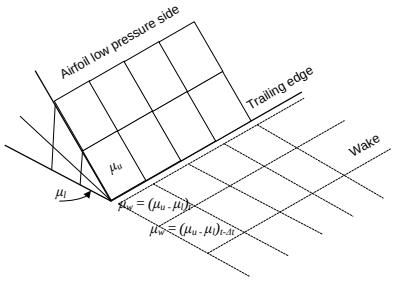

Figure 4: Panel representation of the wing and the release of panels representing the wake.

4 Results

4.1 3D flow field close to the blade

Contour plots for the axial, radial and tangential velocities are shown in figs. 5, 6 and 7 respectively for three spanwise positions of 0.31m, 0.52m and 1m. In each figure the left coloumn shows the experimental results while the right coloumn shows the numerical results. In general, the agreement is very good. Differences arise primarily just behind the trailing edge corresponding to the trailing vorticity sheet. Since the panel model considers the sheet as having zero thickness, the results differ from the experimental ones in this region. This appears clearly at the mid board station of the tangential velocity results in fig. 7. Also some major discrepancies occur again just behind the trailing at the tip region. These are particularly clear in figs. 5 and 6. Both velocity components obtained from the panel model show a sudden flow inversion in a small region just behind the trailing edge. These discrepancies decrease with increasing azimuthal resolution. However, an azimuthal increment of less than 5°would require substantial computational overhead which is not practical.

At the tip, both the axial and radial velocity components increase dramatically but the tangential component becomes small. At the root of the blade (maximum chord region), the radial velocity is very small. This shows that neither the root vorticity nor the nacelle affect this flow component at this 31% span position. This means that in this root region, the outer flow is predominantly 2D. In the midboard region at 52% span, the flow still remains approximately 2D since the spanwise component is still small.

From the SPIV data it was possible to extract the 3D flow field around the blade (in

Table 2: Input parameters for the panel code simulation

	TU Delft	MEXICO
Blade spanwise panels	58	44
Blade chordwise panels	54	32
Nacelle spanwise panels	50	50
Nacelle circumferential panels	50	50
Azimuthal step	5°	5°
No. of rotor revolutions	10	10
Vortex model	Ramasamy-Leishman [15, 16]	
Core growth model	Ramasamy-Leishman [15, 16]	

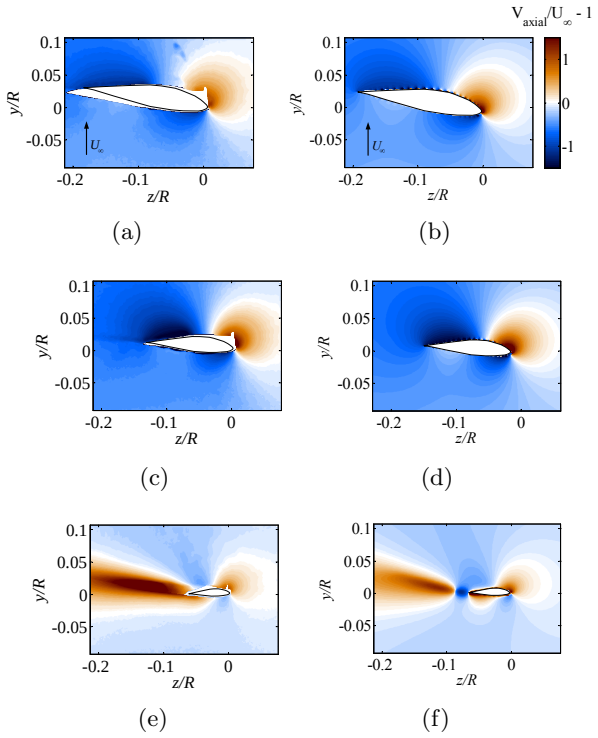

Figure 5: Axial velocity contours as obtained from the SPIV results (left coloumn) and the potential flow panel model (right coloumn) for the TU Delft blade. 5(a) and 5(b) r/R = 0.31, 5(c) and 5(d) r/R = 0.52, 5(e) and 5(f) r/R = 1.

its horizontal position) by interpolating between the measurement planes. The volumetric visualisation of the three velocity components are shown in fig. 8.

4.2 Bound vorticity

The bound vorticity was found from the experimental data by integrating the velocities around a rectangular contour. This integration procedure was carried out for all of the 29 planes and hence a smooth spanwise bound vorticity variation was obtained. The choice of contour size was found to have negligible effect on the calculation of the bound vorticity. Nonetheless it was clear that since there is some uncertainty in the SPIV data, the choice of contour could have

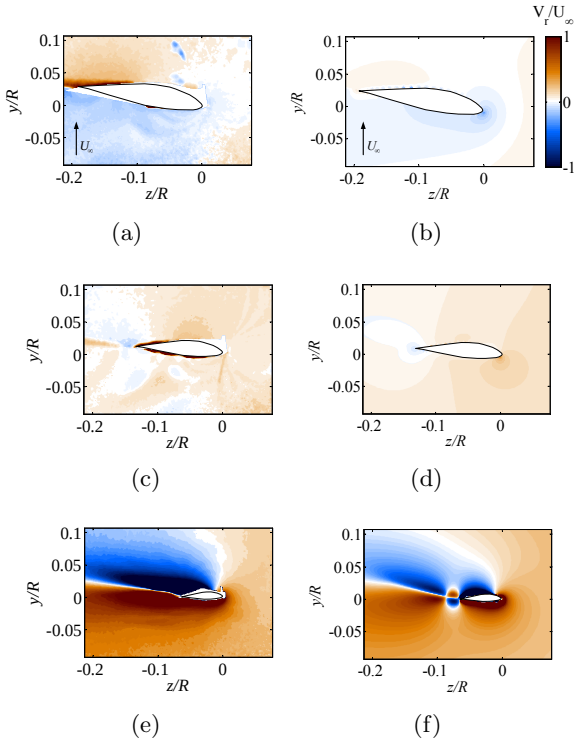

Figure 6: Radial velocity contours as obtained from the SPIV results (left coloumn) and the potential flow panel model (right coloumn) for the TU Delft blade. 6(a) and 6(b) r/R = 0.31, 6(c) and 6(d) r/R = 0.52, 6(e) and 6(f) r/R = 1.

an impact on the total uncertainty in the measurement.

In fig. 9, the bound vorticity is non-dimensionalized and plotted against span position. The results from the 3D potential flow panel model are also plotted for comparison. In the mid-board region of the blade, the numerical and experimental results differ by around 15%. This disagreement can be associated with slight experimental errors in quantities such as blade pitch. Also, the estimation of bound vorticity utilizes a contour which traverses the flow discontinuity caused by the trailing wake vorticity sheet.

4.3 Blade shape and trailing vorticity

The geometries of the TU Delft and MEXICO blades are shown in fig. 10. The blades are scaled down by their radius. The tip speed ratios for the two rotors, although optimal, are slightly different (7 for the TU Delft rotor and 6.67 for the MEXICO rotor).

In fig. 11, a comparison of the normalized trailing vorticity of the TU Delft to that of the MEXICO blade is shown. For the TU Delft rotor both experimental and numerical results are shown. On the other hand, only numerical results are available for the MEXICO rotor. In the root region, the TU Delft rotor shows a negative trailing vorticity associated with a relatively strong root vortex. There is some difference between the experimental and numerical results. The MEXICO rotor exhibits a different root vortex behaviour. A strong, positive vorticity is released at around $r/R = 0.2$ which then goes to negative at the connection point to the hub. Two strong root vortices of opposite orientation therefore result. For both blades, the trailing vorticity in the mid-board is small but not zero. The TU Delft rotor shows a higher trailing vorticity especially towards the tip. As expected, the strength of the tip vortex from the experimental result is quite larger than that predicted numerically. Again however, the

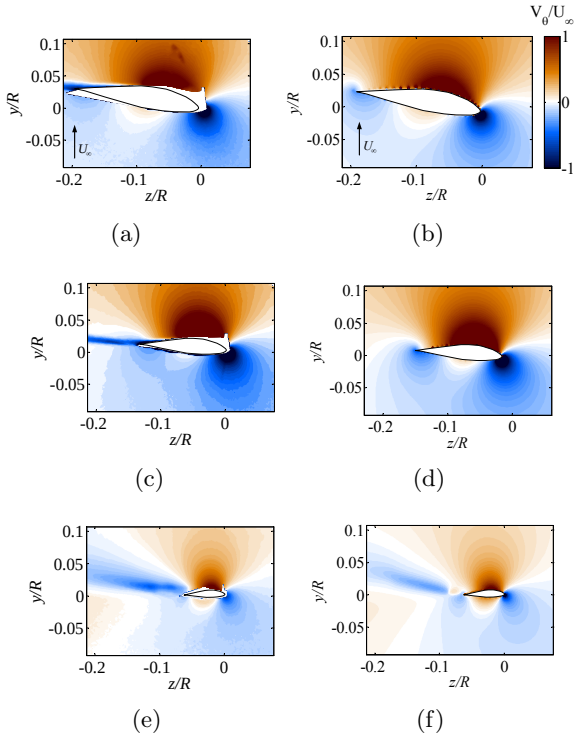

Figure 7: Tangential velocity contours as obtained from the SPIV results (left coloumn) and the potential flow panel model (right coloumn) for the TU Delft blade. 7(a) and 7(b) r/R = 0.31, 7(c) and 7(d) r/R = 0.52, 7(e) and 7(f) r/R = 1.

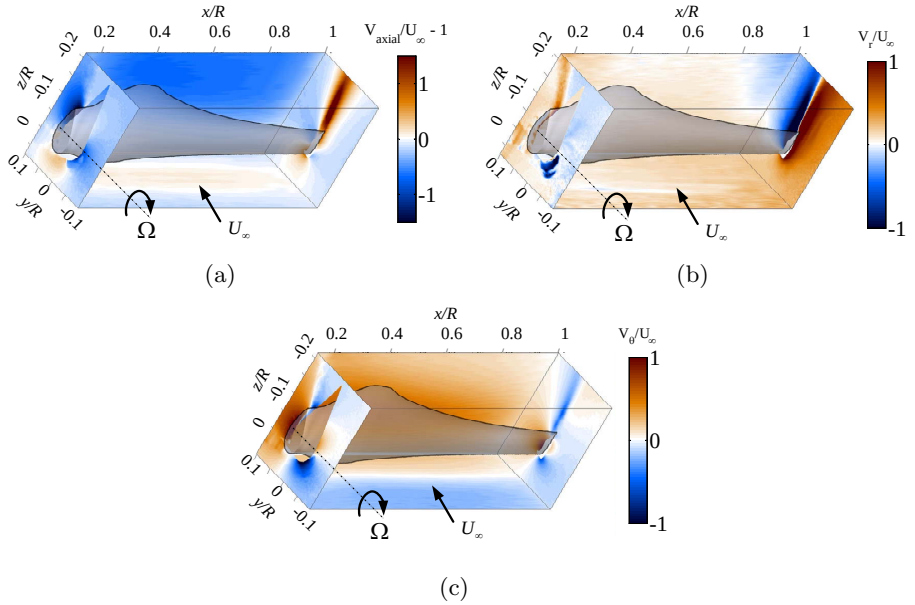

Figure 8: 3D views of the flow field measured around the TU Delft blade.

estimation of the bound vorticity using a simple contour integral at the tip is questionable due to the high flow discontinuity. For the MEXICO blade, due to the tapered tip chord, the trailing vorticity shows a maximum at around $r/R = 0.98$ which then drops substantially at the tip.

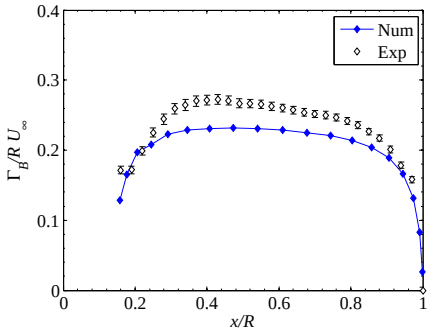

Figure 9: Dimensionless bound vorticity variation with dimensionless radial position. Numerical and experimental results are shown.

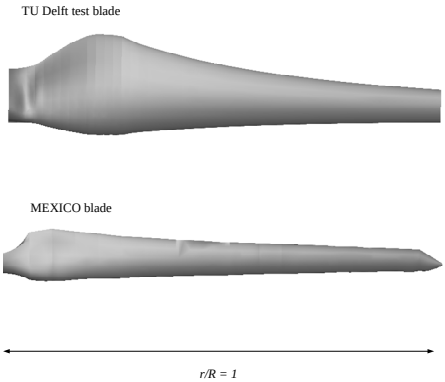

Figure 10: Comparison of the tested TU Delft blade with the MEXICO blade. The blades are scaled according to their radius.

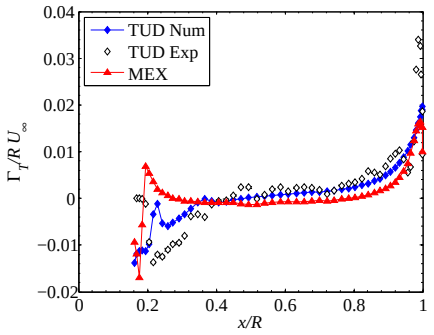

Figure 11: Dimensionless trailing vorticity comparison between the TU Delft and the MEXICO blades. No experimental results for the MEXICO blade are available.

4.4 Separation of body and wake effects for the TU Delft rotor

With the numerical model, it was possible to decompose velocities in those due to the panels which constitute the wake and the velocities due to panels which constitute the bodies which includes the blades and the nacelle. Figs. 12(a), 12(b) and 12(c) show the decomposed axial, radial and tangential velocities. The velocities are shown at the quarter chord blade position at a downstream distance of $y/R = 0.06$. At this position, the agreement between the experimental and numerical results for the axial velocity is very good. The effects of the body panels are

also quite high and cause an induction which is opposite in direction to that due to the wake. At the tip region, a jump in axial velocity due to the body panels may be observed which then reduces to zero for $r/R > 1$. At the root, the numerical results show a dramatic drop in axial velocity which does not compare too well with the experimental observations. These effects can be associated with the inability of the model to predict separation at the connection point of the blade with the hub.

The radial velocities from the experiment show higher velocities at the root compared with the numerical simulations. At the tip, the trends from the numerical and experimental results show the same phenomenon; a drop in the radial velocities. The decomposed results from the numerical model show that this drop is due to the effect of the body panels. The trend due to the wake panels is increasing from root to tip. The resultant is that the radial velocities increase from root to tip but in the tip region the radial flow drops due to the blade effect. This means that the tendency of the blade presence is to cause a reduction in three-dimensionality in the tip zone at the studied downstream position.

The tangential velocities are primarily due to the body effect since the tangential velocity due to the wake panels drop from 0.2 to 0 from root to tip while that due to the body reaches a level of about 0.7 over a large part of the blade. The comparison between the experiment and the numerical results or not as good as the axial velocities but still a strong increase at the root was captured. This increase can also be due to the nacelle effects.

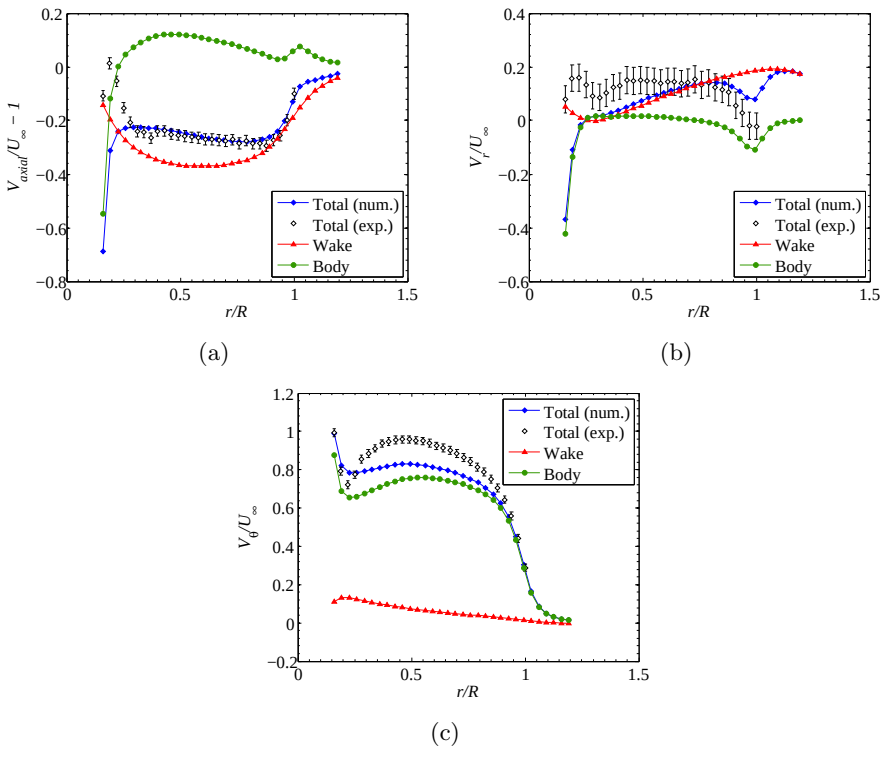

Figure 12: Dimensionless velocity variations along the TU Delft blade at a downstream distance of y/R = 0.06.

4.5 Body and wake effects compared between rotors

In this section, the differences in velocities between the TU Delft and the MEXICO rotor velocities at a downstream distance of $y/R = 0.06$ are investigated by means of the numerical

approach. In fig. 13 the total velocities due to the wake and body panels are compared. In fig. 14, the velocity components due to the effects of the wake panels and the effects of the body panels (nacelle and blades) are compared between the MEXICO and TU Delft blade.

The dimensionless axial inductions shown in fig. 13(a) show some considerable differences. The MEXICO blade shows a larger induction especially towards the tip region. The reasons for these discrepancies can be unveiled from fig. 14(a). The wake induction factors show some differences along the entire blade due to the difference in trailing vorticity mentioned earlier. The inductions due to the body panels cause an axial velocity which is downwind(positive). The MEXICO blade body panels induction is much lower than those for the TU Delft blade. Both of these substantial discrepancies combine to give the differences found in fig. 13(a).

The radial velocities in fig. 13(b)also show similar trends. At the root however, the TU Delft blade shows a high inboard velocity which is not observed on the MEXICO blade. Moreover, the MEXICO blade, due to the tapered tip, shows an increase in radial velocity from root to tip. As opposed to the TU Delft blade, the drop of radial velocity in the tip region is barely noticeable. This leads to the important result that tapered tips lead to a higher radial flow in the tip region, which is not the case for a blunt tip. This outcome will be discussed in future work. In fig. 14(b) the radial inductions due to the wake panels for both the TU Delft and MEXICO rotors agree considerably and an almost linear increase can be observed from root to tip. The major differences are in the effects of the body panels where the radial induction is in the opposite direction (inboard) with respect to the effects of the wake. For the TU Delft rotor this induction is much larger than the MEXICO rotor due to the blunt tip. This is the underlying reason why the MEXICO blade shows a higher three-dimensionality in the tip region (refer to fig. 13(b)).

The tangential flow components of fig. 13(c) highly differ between the TU Delft and the MEXICO blades. The reason for this is that this component, in the blades vicinity, is very sensitive to the blade geometry. Hence differences in airfoil profiles (as is the case with these two rotors) will lead to differences in this velocity which are highly sensitive in this region of the flow. The velocities due to the wake panels show almost complete agreement for both rotors but those due to the body panels differ substantially (see fig. 14(c)). This supports the observations of the combined velocities in fig.13(c).

5 Conclusions

The experimental measurements performed in this study give a deeper insight on the flows around the wind turbine blade as compared to the works of Mast et al. [5] and Maeda et al. [10]. The 3D unsteady, potential-flow panel model was successfully validated and used to give further insight into the flows just downstream of the blade. The investigated hypthesis was confirmed and hence the flow three-dimensionality in the blade vicinity is highly affected by the blade influence not only due to the effects of the released wake but also due to vorticity which is still bound to the blade.

The blade influence was found to distort the flow field generated by the wake and the freestream. Especially in the tip region, flow three-dimensionality cannot be simply considered as occurring due to the tip vortex. The body influence plays a fundamental role for the determination of the extent of this three-dimensionality. The proof of this hypothesis was given by comparing the tested blade with the results for the MEXICO rotor. Due to its tapered tip, the MEXICO rotor exhibits a relatively small blade influence on the radial flow component. On the other hand, the blunt tip of the tested rotor showed strong influence on the radial flow which surprisingly alleviates the three-dimensional effects at the tip.

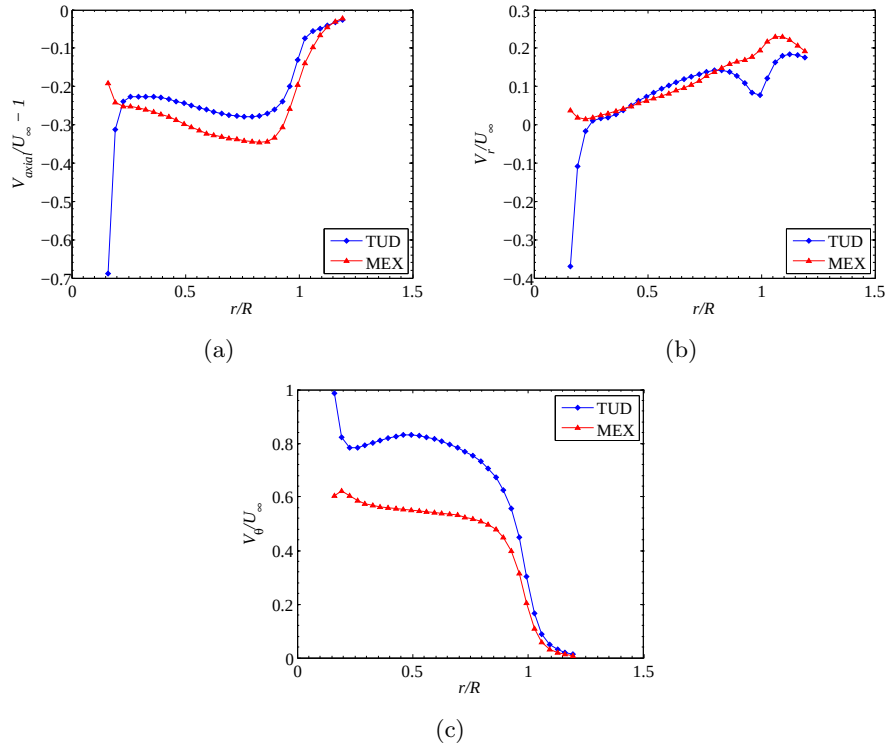

Figure 13: Comparison of the non-dimensionalized velocity components for the TU Delft rotor and the MEXICO rotor at a downstream distance of y/R = 0.06. The velocities shown are due to both the body (nacelle and blades) and the wake panels.

Future work will expand on these conclusions by considering the way in which bound vorticity is distributed over the blade panels. This will enable a better understanding of why bound vorticity causes the velocity components discussed here. Furthermore this will give insight into the wake development in the rotor proximity.

6 Acknowledgment

The research work disclosed in this publication is partially funded by Malta Government Scholarship Scheme grant number MGSS PHD 2008-11, Vestas and TU Delft. The authors also acknowledge the assistance of B. Geurts during the experiment.

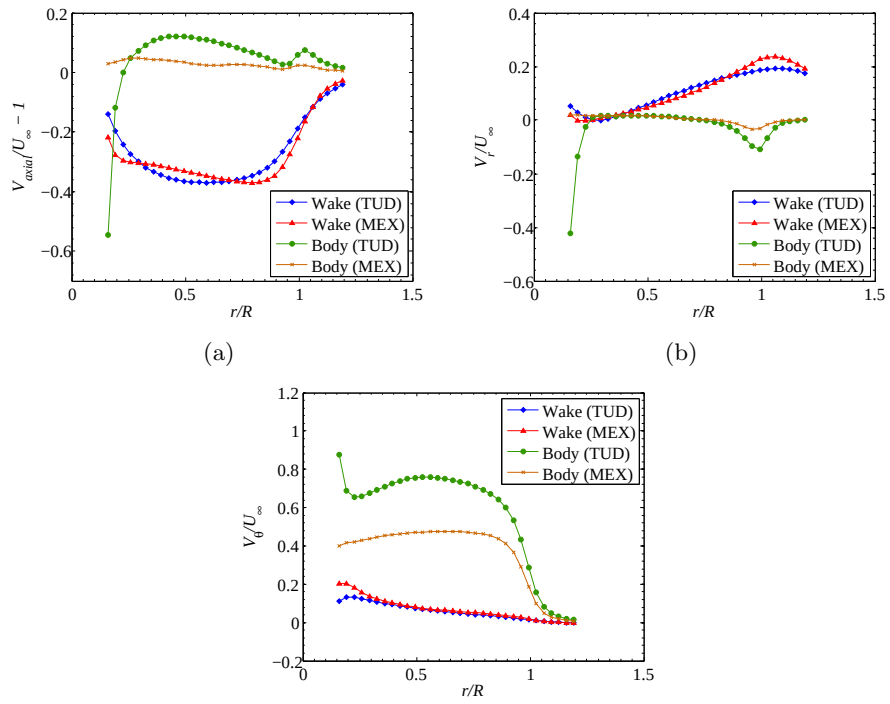

Figure 14: Comparison of the decomposed non-dimensionalized velocity components for the TU Delft rotor and the MEXICO rotor at a downstream distance of y/R = 0.06. The velocities shown are the decomposed values due to the body (nacelle and blades) panels and those due to the wake panels.

References

[1] Betz, A., 1919. "Schraubempropellor mit geringstem energieverlust".

[2] Hand, M., Simms, D., Fingersh, L., Jager, D., Cotrell, J., Schreck, S., and Larwood, S., 2001. Unsteady Aerodynamics Experiment Phase VI: Wind Tunnel Test Configurations and Available Data Campaigns. Technical Report NREL/TP-500-29955, National Renewable Energy Laboratory 1617 Cole Boulevard Golden, Colorado 80401-3393.

[3] Sant, T., van Bussel, G., and van Kuik, G., 2006. "Estimating the angle of attack from blade pressure measurements on the NREL Phase VI rotor using a free wake vortex model: Axial conditions". *Wind Energy Journal*, **9**, pp. 549–577.

[4] Sezer-Uzol, N., and Long, L., 2006. "3-d time-accurate cfd simulations of wind turbine rotor flow fields". In AIAA Paper 2006-394, 44th AIAA Aerospace Sciences Meeting and Exhibit.

[5] Mast, E. H. M., Vermeer, L. J., and van Bussel, G. J. W., 2004. "Estimation of the circulation distribution on a rotor blade from detailed near wake velocities". *Wind Energy Journal*, **7**, pp. 189 – 209.

[6] Medici, D., and Andersson, P., 2006. "Measurements on a wind turbine wake 3d effects and bluff body vortex shedding". *Wind Energy Journal*, **9**, pp. 219 – 236.

[7] Ebert, P., and Wood, D., 1997. "The near wake of a model horizontal-axis wind turbine - i experimental arrangements and initial results". *Renewable Energy,* **12**, pp. 225–243.

[8] Ebert, P., and Wood, D., 1999. "The near wake of a model horizontal-axis wind turbine - ii. general features of the three-dimensional flowfield". *Renewable Energy,* **18**, pp. 513–534.

[9] Ebert, P., and Wood, D., 2001. "The near wake of a model horizontal-axis wind turbine part 3: Properties of the tip and hub vortices". *Renewable Energy,* **22**, pp. 461–472.

[10] Maeda, T., Kamada, Y., Sakai, Y., and Takahara, N., 2004. "Wind tunnel study of the flow field around the blade of a HAWT". In EWEA - 2004 European Wind Energy Conference.

[11] Schepers, J. G., and Snel, H., 2007. Model experiments in controlled conditions(MEXICO), June. ECN-E-07-042.

[12] Katz, J., and Plotkin, A., 2001. *Low-Speed Aerodynamics*, second ed. Cambridge University Press.

[13] Dixon, K., 2008. "The near wake structure of a vertical axis wind turbine". Master's thesis, Technische Universiteit Delft.

[14] Ferreira, C. S., 2009. "The near wake of the vawt". PhD thesis, Technische Universiteit Delft.

[15] Ramasamy, M., and Leishman, J. G., 2006. "A generalized model for transitional blade tip vortices". *Journal of the American Helicopter Society,* **51**(1), pp. 92–103.

[16] Ramasamy, M., and Leishman, J. G., 2007. "A Reynolds number-based blade tip vortex model". *Journal of the American Helicopter Society,* **52**(3), pp. 214–223.